



**HAL**  
open science

## Evaluation of core–shell poly(vinylidene fluoride)-grafted-Barium titanate (PVDF-g-BaTiO<sub>3</sub>) nanocomposites as a cathode binder in batteries

Fatima Ezzahra Bouharras, Mustapha Raihane, Mohamed Baccour, Nicolas Louvain, Bruno Ameduri

► **To cite this version:**

Fatima Ezzahra Bouharras, Mustapha Raihane, Mohamed Baccour, Nicolas Louvain, Bruno Ameduri. Evaluation of core–shell poly(vinylidene fluoride)-grafted-Barium titanate (PVDF-g-BaTiO<sub>3</sub>) nanocomposites as a cathode binder in batteries. *Solid State Ionics*, 2020, 356, pp.115441. 10.1016/j.ssi.2020.115441 . hal-02949281

**HAL Id: hal-02949281**

**<https://hal.science/hal-02949281>**

Submitted on 23 Sep 2022

**HAL** is a multi-disciplinary open access archive for the deposit and dissemination of scientific research documents, whether they are published or not. The documents may come from teaching and research institutions in France or abroad, or from public or private research centers.

L'archive ouverte pluridisciplinaire **HAL**, est destinée au dépôt et à la diffusion de documents scientifiques de niveau recherche, publiés ou non, émanant des établissements d'enseignement et de recherche français ou étrangers, des laboratoires publics ou privés.



Distributed under a Creative Commons Attribution - NonCommercial 4.0 International License

## Evaluation of core–shell poly(vinylidene fluoride)-*grafted*-Barium titanate (PVDF-*g*-BaTiO<sub>3</sub>) nanocomposites as a cathode binder in batteries

Fatima Ezzahra BOUHARRAS,<sup>a,b</sup> Mustapha RAIHANE,<sup>a</sup> Mohamed BACCOUR<sup>b</sup> Nicolas LOUVAIN,<sup>\*,b,c</sup> and Bruno AMEDURI<sup>b</sup>

<sup>a</sup> IMED-Lab, Faculty of Sciences and Techniques. Cadi Ayyad University (UCA), Av. A. El Khattabi, B.P. 549, 40000, Marrakesh, Morocco

<sup>b</sup> ICGM, Univ. Montpellier, CNRS, ENSCM, Montpellier, France

<sup>c</sup> Réseau sur le Stockage Electrochimique de l'Energie (RS2E), FR CNRS 3459, Hub de l'Energie, Amiens, France

\*nicolas.louvain@umontpellier.fr

### Abstract

Poly(vinylidene fluoride)-*grafted*-Barium titanate (PVDF-*g*-BaTiO<sub>3</sub>) nanocomposites were used as binders to prepare cathode material containing 70 wt.% of active material (LiMn<sub>2</sub>O<sub>4</sub>), 18 wt.% of conducting agent (carbon black) and 12 wt.% of binder (either commercially available PVDF, modified PVDF such as PVDF-*g*-BaTiO<sub>3</sub>, or both). A calendaring process was used in order to obtain homogenous films and a better dispersity of nanoparticles. First, the electrochemical behavior of the modified PVDF was explored in the absence of the active material and did not revealed any electrochemical activity. Then, after adding the active material into the formulation (4-12 wt.%), cells made with commercially available PVDF displayed similar cycling performances as the one achieved from 4 wt.% of modified PVDF. For example, at 1C, the initial discharge capacities were 146, 140 and 130 mA h g<sup>-1</sup> for films made by 0, 4 and 8 % of modified PVDF, respectively. Moreover, with the increase of charge discharge rate to 10 C, the capacity can be approximately recovered when the current density returned to 1 C for all the samples, revealing a good reversibility of the structure. On the other hand, calendaring procedure enables to obtain a uniform structure demonstrated by reproducible tests as compared to those achieved from non-calendered films. Moreover, the calendaring process showed an enhancement

in cycling performances. For instance, the initial discharge capacity at 1 C was 124 and 108 mA h g<sup>-1</sup> and decreased to 82 and 2 mA h g<sup>-1</sup> at 10 C for non-calendered and calendered sample made with commercial PVDF, respectively.

**Keywords:** PVDF, nanocomposites, energy, calendering.

## 1. Introduction

The increasing number of electronic devices represents a challenge for the industry. Actually, the design of a passive electronic component having high performances with moderate production costs, light weight and small size requires great efforts in the field of research and development [1–3]. Actually, polymer nanocomposite systems have attracted significant attention in the recent years due to their wide range use in electronic industry, such as optics, micro-electronics, multilayers, embedded and high energy density capacitors [4–8]. Another important application of polymer nanocomposites deals with lithium ion batteries [9,10]. Having a great potential to achieve very high energy density and low environmental impact, lithium ion batteries become the most used secondary rechargeable storage systems [11–13].

A typical electrode fabrication consists on the active material, a conductive agent, a binder and the solvent that are mixed to form a slurry. This later is then casted onto an aluminum or copper foil and dried at room temperature to yield the electrode. In order to remove all the remaining solvent(s), the prepared electrode is further dried under vacuum before making the cell.

To enhance the battery performances, several studies have been reported on active material, binder or even electrolyte, in which polymer nanocomposites have been widely used [14,15]. For example, Kumar *et al.* [16] used BaTiO<sub>3</sub> as a filler in poly(VDF-HFP) copolymer based composite solid polymer electrolyte (CSPE) prepared by solution casting. The results show that the highest DC conductivity reached  $2.19 \times 10^{-6} \text{ S cm}^{-1}$  at 300 K, which increased to  $8.89 \times 10^{-6} \text{ S cm}^{-1}$  after adding 4 wt.% of BaTiO<sub>3</sub>. Other works have also reported the usefulness of other kinds of fillers [17,18]. Meneghetti and Qutubuddin [17] synthesized polymer-clay nanocomposites and tested them as possible candidates as electrolytes in lithium-ion cells. The obtained films displayed excellent mechanical strength with conductivity comparable as more traditional polymer electrolytes made with added lithium salts. Ferrari *et al.* [18] reported different types of fillers (*e.g.*, ceramics, metal oxides, glass...) that can be incorporated into the polymer matrix or formed in situ by different synthetic strategies.

On the other hand, and although they are electrochemically inactive material, the binder can have a significant influence on the electrode performance at both macroscopic and microscopic levels [3,14,19]. The former is associated to the electrochemical performances, while the second one concerns the interactions of the polymer binder with the different battery components (*i. e.*, active material, conductive agent and electrolyte). Choi *et al.* [20] showed that the increase in the binder content and the binder/electrolyte affinity led to an increase in the electrode ionic

conductivity. Moreover, they pointed out the effect of the binder species on the electrochemical performances since the absorbed amount of electrolyte into the cathode depends on the nature of the binder. In fact, various kinds of binders have been attempted, such as poly(vinyl acetate) [21], poly(vinyl alcohol) [22], poly(acrylic acid) [23], poly(methyl methacrylate) [24], carboxymethyl cellulose [14] and natural cellulose [25]. Besides the listed polymers, polyvinylidene fluoride, PVDF, and its blend copolymers are considered to be the most common and widely used binder material in lithium ion batteries, thanks to their good electrochemical and thermal stability as well as its strong adhesion properties [24,26,27]. However, it is believed that PVDF properties could be further improved (*e.g.*, increasing both its mechanical properties and electrochemical stability and decreasing its crystallinity) by grafting it with other species in order to improve overall electrode properties [3]. Zheng *et al.*[28] studied the effect of PVDF modified with blending copolymer polyethylene-*block*-poly(ethylene glycol) copolymer and poly(propylene carbonate)s, used as binder material using LiCoO<sub>2</sub> as active material and carbon black as conductive agent. It was found that the modified PVDF improves the dispersion of carbon black compared to the pure PVDF binder, leading to an enhanced uniformity of the electrode composite.

Apart from the polymer binder nature, molar mass of the used polymer is also an important factor. Wang *et al.*[29] investigated the effect of the molar mass of PVDF binder on the electrochemical performances of LiNi<sub>0.33</sub>Co<sub>0.33</sub>Mn<sub>0.33</sub>O<sub>2</sub> (NMC) electrodes made by a dry powder coating process. The authors found that the PVDF formed a thin layer around the NMC particles surface after heating it to above its melting temperature, and by increasing the molar mass of the polymer, the PVDF layer became more porous, thus improving the high rate capacity of the electrodes. Wang *et al.* [30] also studied the effect of PVDF molar mass on the electrode performances using a wet-slurry procedure. In contrast to Wang *et al.*'s strategy [29], they found that the lowest molar masses favored the best performances.

In this work, modified PVDF was used to prepare electrodes based on LiMn<sub>2</sub>O<sub>4</sub> as the active material and carbon black as the conductive agent. This binder, named as PVDF-*g*-BT, was obtained from a reversible addition fragmentation chain transfer polymerization (RAFT) of VDF from the surface of BaTiO<sub>3</sub> nanoparticles decorated with xanthate functions, leading to a well-structured nanocomposite materials. The electrochemical tests, including cyclic voltammetry, charge-discharge capacity and rate performance were investigated on the prepared cells.

## 2. Experimental section

## 2.1 Materials

The binders tested are commercially available polyvinylidene fluoride (Solef® 5130/1001 PVDF, vinylidene fluoride, homopolymer, > 99.9 %) purchased from Solvay and modified PVDF-*grafted*-Barium titanate (PVDF-*g*-BT) nanocomposites filled with 5 wt% of BaTiO<sub>3</sub>. PVDF-*g*-BaTiO<sub>3</sub> nanocomposites were synthesized by RAFT polymerization of VDF in the presence of BaTiO<sub>3</sub> bearing xanthate group (Schemes S1-S2, the NMR spectra of which are displayed in Figures S1-S2) [31]. Briefly, the first step of Scheme S1 is the hydroxylation of pristine BaTiO<sub>3</sub> using Hydrogen peroxide at 105 °C. The hydroxylated BaTiO<sub>3</sub> (BT-OH) was functionalized by a RAFT agent (xanthate) in two steps (reactions (2) and (3), Scheme S1). Initially, the surface of the BT-OH nanoparticles was modified by the condensation reaction of 3-chloropropyltriethoxysilane (BT-CPTS) in the presence of toluene/water mixture at 80 °C, and it was subsequently reacted in the second step with potassium xanthogenate at 80 °C to produce nanoparticles bearing RAFT xanthate (BT-XA) in the presence of ethanol. All steps led to high yields. In the last step of Scheme S1, the PVDF-*g*-BaTiO<sub>3</sub> core-shell nanocomposites were prepared by RAFT polymerization of VDF at 65 °C in the presence of BT-XA using *tert*-butyl peroxyvalate (TBPPi) as the initiator and dimethyl carbonate as the solvent. At the end of polymerization reaction, the obtained nanocomposites were subjected to several washing treatments using acetone in order to remove all the unattached polymer. The PVDF grafting yields are reported in Table S1 [31].

The active material LiMn<sub>2</sub>O<sub>4</sub> was obtained from Targray. Lithium metal ribbon (Li, 99.9 % trace metal basis) and 1-methyl-2-pyrrolidinone (NMP) (anhydrous, 99.5 %) were purchased from Sigma-Aldrich. Carbon black Super C65 was supplied from Imerys Graphite & Carbon. GE Healthcare Life Sciences Whatman Grade GF/D glass microfiber filters (borosilicate; Ø 55 mm, 675 µm thickness) were procured from Sigma-Aldrich. LiPF<sub>6</sub> 1 M in EC:DMC (1:1 vol.%) electrolyte (99.9 %, H<sub>2</sub>O < 20 ppm) was purchased from Solvionic (Toulouse, France). Except if explicitly noted, all syntheses, materials storages, sample preparations for characterization, and experiments were carried out in an inert atmosphere and/or prepared in a glovebox (H<sub>2</sub>O < 0.5 ppm, O<sub>2</sub> < 0.5 ppm).

## 2.2 Electrodes and coin cells preparation

The cathode films were prepared using 70 wt% LiMn<sub>2</sub>O<sub>4</sub>, 18 wt% of Carbon black (C65), 12 wt% of the binder (PVDF or PVDF-*g*-BT nanocomposite or both) (Table 1).

**Table 1.** Formulations used to prepare electrode materials for batteries with active material.

<i>Formulations (% BaTiO<sub>3</sub> in the composite)</i>	<i>PVDF Wt%</i>	<i>PVDF-g-BT Wt%</i>
0	12	0
4	8	4
8	4	8
12	0	12

To form the slurry, the precursors were homogenized in an agate pestle. After several minutes of blending with a mortar, the mixture was transferred to an agate ball-milling jar (with four balls) (Figure S3a) and 1-methyl-2-pyrrolidinone (NMP) was added. The mixture was then ball-milled softly at 500 rpm for 30 min. The obtained slurry was spread uniformly on aluminum metal grade foil (0.018 mm, Goodfellow) casted by a four-sided film applicator (150  $\mu\text{m}$ ) from Elcometer (Figure S3b). After 48 h of drying at room temperature, the casted films were further dried under dynamic vacuum at 80 °C and -0.850 bar relative pressure in an XFL020 drying oven, France Etuves. In order to enhance the dispersity of the precursors, the dried films were calendered at 50 °C at 5 rpm, where the thickness, understood as the distance between the two rolls, was fixed at 30  $\mu\text{m}$  (Figure S3c), then punched to discs of 12.7 mm in diameter. 316 L stainless steel 2032 coin-cells were used to characterize the positive electrode material under argon atmosphere in a glovebox. To assemble the coin-cell, a spring was placed on the small lid first in order to maintain battery pressure, then lithium foil, which was punched to discs with 14 mm in diameter and already positioned on a thick spacer that plays the role of current collector from the anode side was sited. The electrolyte was dropped on the separator (16 mm, Whatmann GF/D) and the prepared electrode was then placed with its aluminum surface in contact with the coin cell big lid. In the last step, the coin cell was sealed by a crimping machine.

PVDF-g-BaTiO<sub>3</sub> nanocomposite filled with 5 wt.% BaTiO<sub>3</sub> was used as binder material in Lithium ion batteries to test its effect on the electrochemical behavior.

To obtain uniform thicknesses, better particles dispersion and connections and thus a homogeneous structure, a film calendering process was adopted (Figure S3). Such a calendering process consists in placing the casted film or the electrode between two rolls working in opposite directions, where the gap size is significantly smaller than the electrode thickness in order to insure the desired compaction of the electrode coating [32].

This technique was found to enhance not only the mechanical and physical characteristics, but also the electrochemical performances of the electrode [33]. Indeed, it is believed that the calendaring enables to increase the contact between particle to particle and particle to current collector in the electrode, leading to an improvement in both electrical and thermal conductivities [34]. Thicknesses of the films were measured before and after calendaring by picking six different points (Three measurements on the border and three in the middle of each film) as shown in Figure S3b. Table 2 displays the average thicknesses of the electrodes before and after calendaring. Zheng *et al.*[35] studied the effect of calendaring on the morphology of cathode laminates based on Li [Ni<sub>1/3</sub>Mn<sub>1/3</sub>Co<sub>1/3</sub>]O<sub>2</sub>, 8 %wt of PVDF and 7 %wt of acetylene black and they compressed the prepared films to the desired thickness corresponding to the searched porosity, which was adjusted from the free standing (50 %) to 40, 30, 20, 10 and 0 %. These authors found that for the sample having 50 % of porosity, SEM images revealed the presence of several pores and micro-fractures. However, when the porosity was fixed at 30 %, the morphology changed and since the material was not crashed by calendaring, the decrease of film thickness was attributed to the shrinkage of the inactive polymer material.

**Table 2.** Average thicknesses of the different electrodes before and after calendaring in  $\mu\text{m}$  and the Elastic Recovery (ER) determined according to equation 1.

<i>Formulations</i> <i>(% BaTiO<sub>3</sub> in</i> <i>the composite)</i>	<i>Before calendaring</i> ( $\mu\text{m}$ )	<i>After calendaring</i> ( $\mu\text{m}$ )	<i>Elastic recovery (ER)</i>
0	49.5	45.0	0.30
4	46.7	44.3	0.31
8	46.3	37.3	0.16
12	44.5	36.8	0.15

### 2.3. Electrodes characterization and electrochemical measurements

The microstructure of the prepared electrodes (calendered and non-calendered) was observed using a scanning electron microscope (SEM, Zeiss HD15). Cyclic Voltammetry was performed on a VSP instrument at room temperature from 3.2 V to 4.5 V at a scan rate of 0.5 mV s<sup>-1</sup>. Galvanostatic electrochemical characterizations were performed on a BCS-805 battery cycler from BioLogic and BTS 4000 battery testing system from Neware. Measurements were

performed in the voltage range of 4.5-2.5 V vs Li<sup>+</sup>/Li at different current densities. The theoretical specific capacity C of LiMn<sub>2</sub>O<sub>4</sub> was considered equal to 148 mA h g<sup>-1</sup>, for a 1-e<sup>-</sup> process. All current densities were calculated as C\*n for a charge/discharge with n lithium ions (de)inserted in 1 h. The polarisation was calculated as the difference between the average charge and discharge voltage measured at half-charge/half-discharge capacity (E<sub>1/2</sub>). The C-rate measurements were performed by increasing the current densities from 1 C to 10 C step-by-step at 2 C, 4 C, 6 C, and 8 C; before incrementing the current value, a step at 1 C was performed to check if the initial average capacity was recovered.

### 3. Results and discussions

In the present work, electrodes were prepared with a cathode material as active material, a commercially available PVDF or a BaTiO<sub>3</sub>-*grafted*-PVDF binder, a carbon additive, and calendered before assembling coin cells. As well-known, the calendaring procedure is used to adjust electrode porosity and enhances electrical inter-particles and particle-to-current collector contacts, and it globally leads to a higher adhesion and cohesion of active layer to the current collector. Improving electrode porosity has a significant influence on current-rate capability for a given electrode material. It enables to decrease the thickness of the prepared films by 4.5, 2.3, 9.0 and 7.7 μm for formulations made by 0, 4, 8 and 12 wt.% of modified PVDF, respectively. It is worth mentioning that the thickness of the calendered films is still higher than that of the distance between the rolls fixed at 30 μm, and this can be explained by the elastic recovery (ER) of the electrode when the pressure is removed, determined from equation (1):

$$ER = \frac{e_f - e_r}{e_i} \quad (1)$$

where  $e_f$ ,  $e_r$  and  $e_i$  stand for the final, in-between the roll and initial thicknesses, respectively [34].

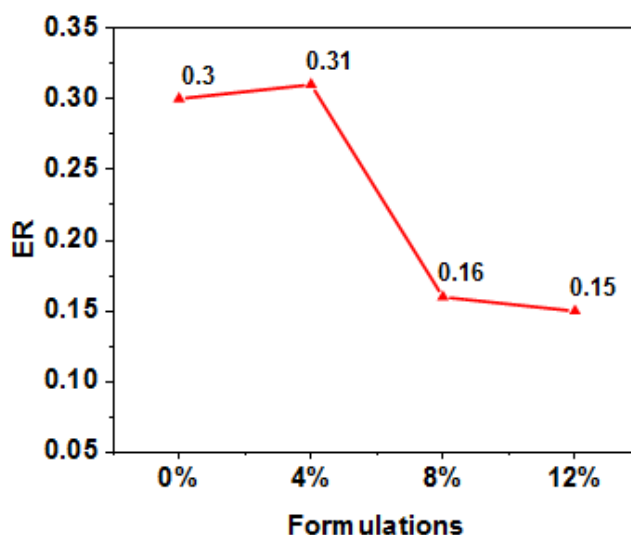


**Figure 1.** Elastic recovery (ER) determined from equation (1), for different formulations based on the active material.

From Figure 1, the elasticity of the films decreases as the feed amount of modified PVDF in the formulation increased. For instance, the ER decreased from 0.3 for formulation made from commercially available PVDF to 0.15 when modified PVDF (12 wt.%) was used. This variance comes from the difference in PVDF structure and namely in molar masses. In fact, the commercially available PVDF presents a molar mass of approximately  $1,200,000 \text{ g mol}^{-1}$ , higher than that of the modified one (ca.  $3,300 \text{ g mol}^{-1}$ ) [31], thus carrying long polymer chains. Those latter confine to the film an elastic deformation that dominates the densification process when the calendaring is applied, leading to increased elastic recovery (ER).

In order to further explore the influence of modified PVDF on electrode, the films were characterized by scanning electronic microscopy (SEM). Figure 2 exhibits the SEM images of non-calendered (0NC %) and calendered films (0, 4, 8 and 12 %).

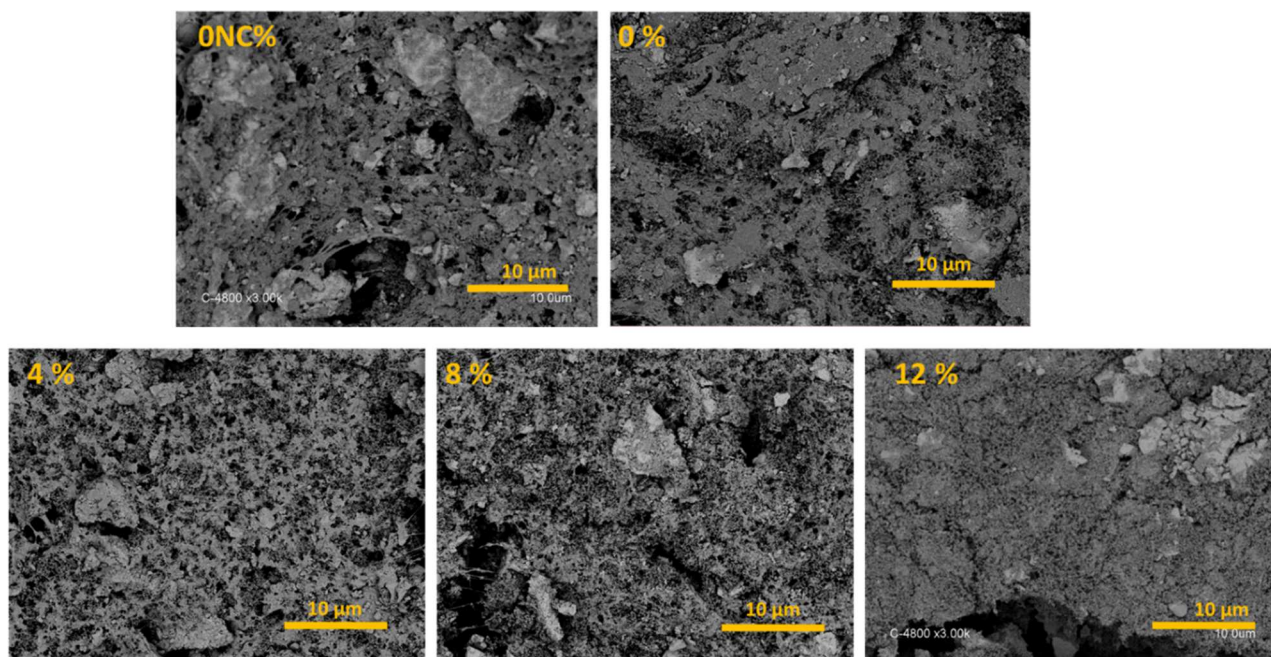


**Figure 2.** SEM images of non-calendered (0NC %) and calendered films (formulations 0, 4, 8 and 12 %).

The SEM images of the electrode made from commercial PVDF confirm that the calendering procedure induces an optimization of the electrode porosity with less voids (0NC% vs 0% samples, Figure 2). In all samples, particles are well dispersed in the film and it is worth noting the presence of some aggregates that could be related to  $\text{LiMn}_2\text{O}_4$ . After calendering the sample with 0 % of modified PVDF, the obtained film presents a softer surface as compared to that of the non-calendered one. With 8 and 12 wt.% of oxide-grafted PVDF, the film surface presents cracks that could originate from the low molar mass of modified PVDF (Figure S4). Another reason for the presence of such cracks could be due to the high crystallinity of the prepared PVDF ( $\chi=48\%$  [31]) compared to commercial one where  $\chi$  varies between 38 and 46 % [36]. Indeed, the binder is responsible to bind all the particles together on the current collector. If the polymer binder molar mass is too low, it might result in a cracked surface as seen in Figure S4. The presence of cracks might also provide an improved electrolyte access to the active material, enhancing the electrochemical properties. It is believed that calendering procedure renders the structure of the film more compact and thus reduces the pores and voids leading to enhanced electrochemical performances.

To compare the electrochemical behavior of the prepared cells made from the active material, cyclic voltammetry measurements were conducted at a scan rate of  $0.5 \text{ mV s}^{-1}$  between 3.2 and 4.5 V vs  $\text{Li}^+/\text{Li}$  (Figure 3).

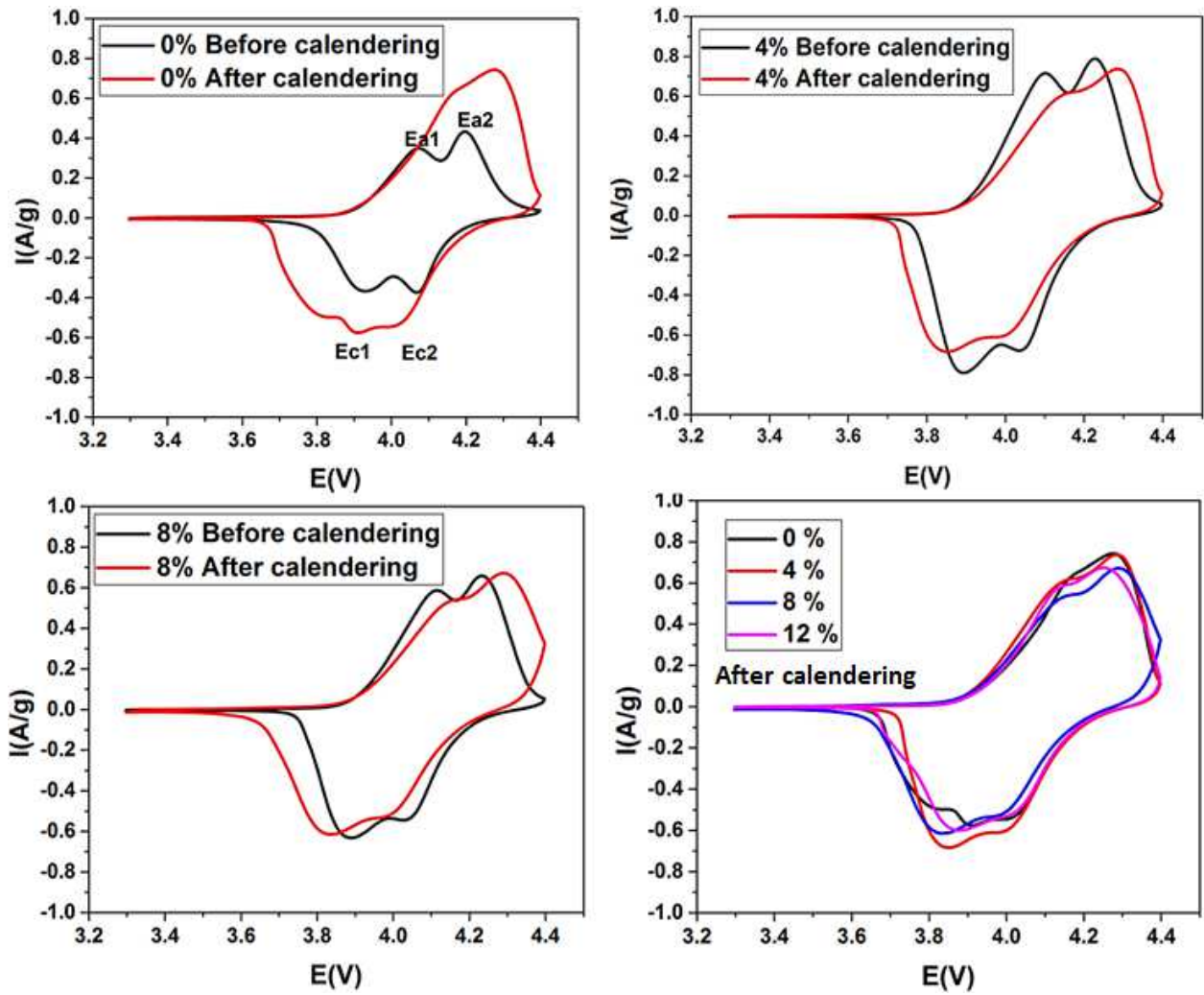


**Figure 3:** Cyclic voltammograms of the prepared cells using LMO as active material performed at a scan rate of 0.5 mV/s, where  $E_{a1}$  and  $E_{a2}$  refer to the potentials at the first and second anodic peaks, respectively; while  $E_{c1}$  and  $E_{c2}$  stand for the potentials at the first and second cathodic peaks, respectively.

For all formulations, and before calendaring, two pairs of separated redox peaks are observed: two oxidation peaks located at about 4.1 V and 4.2 V, and two reduction peaks at about 3.9 V and 4.04 V, characterizing lithium ions extraction-insertion from-into the tetrahedral sites of  $\text{LiMn}_2\text{O}_4$  [37]. In fact, the first peak is attributed to the removal of  $\text{Li}^+$  from half of the spinel framework where Li-Li interactions exist ( $\text{LiMn}_2\text{O}_4/\text{Li}_{0.5}\text{Mn}_2\text{O}_4$ ), while the second peak is assigned to the  $\text{Li}^+$  removal from the other tetrahedral sites ( $\text{Li}_{0.5}\text{Mn}_2\text{O}_4/\gamma\text{-MnO}_2$ ) in which such an interaction does not exist [37–39]. However, after the calendaring procedure, it is observed that: i) the separation between two redox pairs became less discernable; ii) a higher peak current was obtained after calendaring which is more prominent in the 0% sample and iii) the  $\Delta E$  (separation between  $E_a$  and  $E_c$ ) became more important (Table 3). Assuming that the

intercalation reaction is controlled by the solid-state diffusion of Li<sup>+</sup>, the diffusion coefficient could be determined from the peak current  $I_p$  intensity using the following equation [40,41] :

$$I_p = 2.69 \times 10^5 \times n^{3/2} \times A \times D_{Li}^{1/2} \times v^{1/2} \times C_{Li}^0 \quad (2)$$

where  $v$  stands for the scan rate,  $n$  the number of electrons per reaction species ( $n \sim 1$  for LiMn<sub>2</sub>O<sub>4</sub>),  $A$  the surface area of the electrode while  $C_{Li}^0$  represents the bulk concentration of Li<sup>+</sup> in the electrode (given as 0.02378 mol cm<sup>-3</sup> from the theoretical density of spinel).

**Table 3.** Summary of CV results at the potential scanning rate of 0.5 mV/s and the determined diffusion coefficients ( $D_{a1}$  and  $D_{a2}$ ) before and after calendaring.

	Before calendaring				After calendaring			
	$\Delta E_a$ (V)	$\Delta E_c$ (V)	$D_{a1}$ ( $10^{-9} \text{ cm}^2 \text{ s}^{-1}$ )	$D_{a2}$ ( $10^{-9} \text{ cm}^2 \text{ s}^{-1}$ )	$\Delta E_a$ (V)	$\Delta E_c$ (V)	$D_{a1}$ ( $10^{-9} \text{ cm}^2 \text{ s}^{-1}$ )	$D_{a2}$ ( $10^{-9} \text{ cm}^2 \text{ s}^{-1}$ )
0%	0.14	0.12	3.70	5.65	0.26	0.27	11.80	16.90
4%	0.21	0.19	15.30	17.00	0.30	0.29	11.50	16.70
8%	0.23	0.19	9.15	1.31	0.32	0.32	8.72	13.60
12%	-	-	-	-	0.26	0.22	10.10	13.60

From Table 3, it can be noted that the calendaring procedure enables to enhance the diffusion coefficient of Li<sup>+</sup> ions for cells made by 0% of modified PVDF. For instance, the diffusion coefficient at the first anodic peak in 0% sample was  $3.70 \times 10^{-9} \text{ cm}^2 \text{ s}^{-1}$ , and slightly increases to  $1.18 \times 10^{-8} \text{ cm}^2 \text{ s}^{-1}$  after calendaring the film and this matches with the diffusivities obtained in literature [42]. After adding 4% of modified PVDF into the formulation, the diffusion coefficient was found to increase for non-calendered films and decrease after the calendaring process. While after inserting 8% and 12% of modified PVDF, the diffusion was lower.

To further investigate the effect of modification of PVDF with BaTiO<sub>3</sub> nanoparticles on the electrochemical performances of the films, four electrodes were processed from each formulation, and the effect of the modified PVDF was studied. The cells were charged and discharged for 55 cycles from 4.5 to 2.5 V vs Li<sup>+</sup>/Li at various current densities, and the current rate was increased from 1 C to 10 C (more details are supplied in the experimental section). The comparison of the cycling performance of the calendered films at different charge and discharge rates is depicted in Figure 4 and Figures S5-S6.

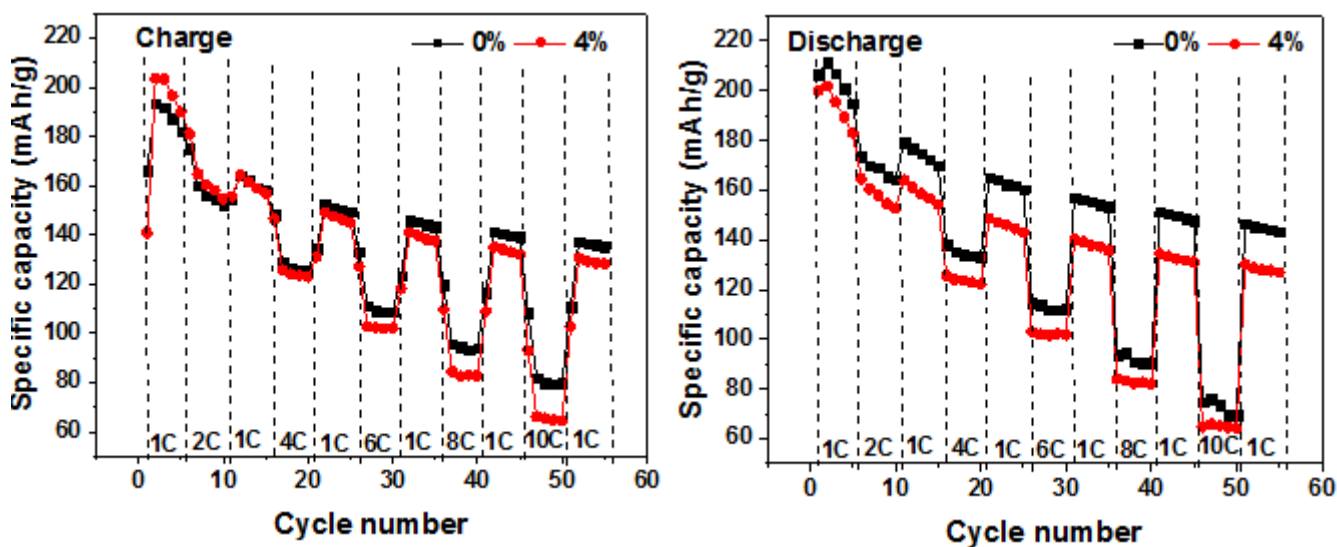


**Figure 4.** Charge and discharge capacities *versus* cycle number for calendered films (0 and 4%). The cycling performance established in the voltage range of 4.5-2.5 V vs Li<sup>+</sup>/Li.

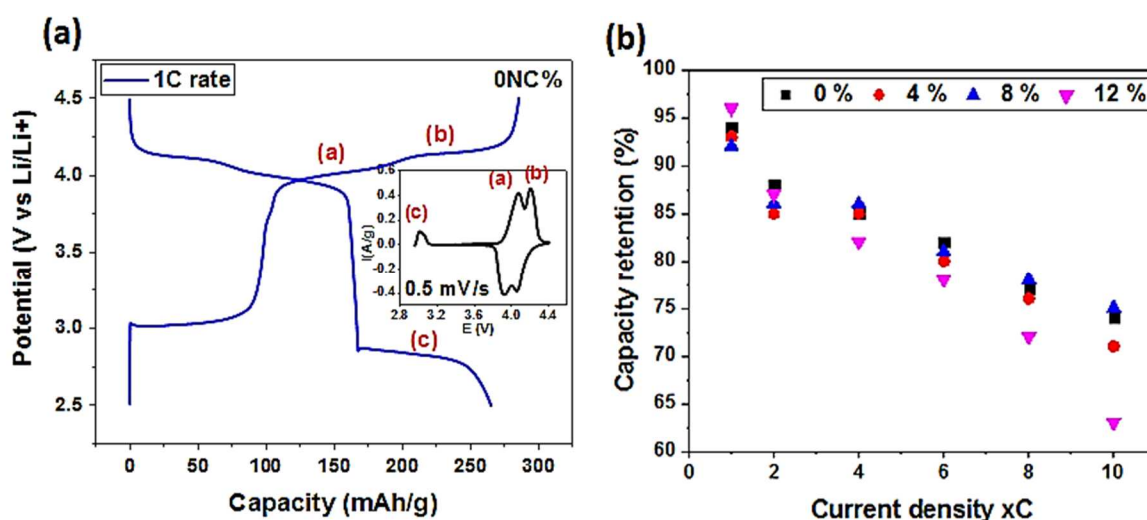
It is worth mentioning that the calendaring process enables to obtain a uniform structure, and this is well noted in the repeatability tests performed on the different cells prepared with disks coming from the same electrode film (Figure S5). Besides the reduction of volumetric density of the electrode film, the calendaring process influences other physical properties, including the interparticle contacts. Thus, the enhancement seen in cycling performance after calendaring procedure could be explained by the increased ohmic contact area at the electrode-current collector interface [43].

Figure 4 exhibits the specific charge and discharge capacities as a function of the number of cycles for formulations 0% and 4%, as extracted from the galvanostatic (i.e. at constant current) curves in charge, or oxidation, and discharge, or reduction (one example of a typical galvanostatic cycle is provided in Figure 5a).

It is observed that as the C-rate increases, a sharp decrease is noted in the specific capacities of the prepared cells. For instance, for 0% sample at 1 C, the discharge capacity is 206 mA h g<sup>-1</sup> and decreases as the current rate increases to 173, 137, 114, 94 and 73 mA h g<sup>-1</sup> at 2 C, 4 C, 6 C, 8 C and 10 C, respectively. This fading of capacity could be attributed to the structural change of the LiMn<sub>2</sub>O<sub>4</sub> spinel due to Jahn-Teller effect and the loss of the active material with dissolution of Mn<sup>2+</sup> into electrolyte [44]. However, even with the increase of charge-discharge rate to 10 C,

the capacity can be approximately recovered when the current density returned to 1 C for all the samples, revealing the good reversibility of the structure.

Furthermore, it is observed that the specific capacity at 1 C and 2 C is higher than the expected one for all samples (Figure 4 and Figure S6), considering only one lithium insertion. This could have two origins: it might be explained by the capacitive behavior of nanosized electrode materials [45,46], or most probably, by the insertion of extra  $\text{Li}^+$  ions into the interstitial octahedral vacant sites of  $\text{LiMn}_2\text{O}_4$  yielding  $\text{Li}_{1+x}\text{Mn}_2\text{O}_4$  (with  $x \leq 2$ ; for  $x = 2$ , the theoretical capacity would be equal to  $296.5 \text{ mAh g}^{-1}$ ), alongside an irreversible phase transition from cubic to tetragonal leading to capacity fading [45,46]. This is evidenced by the two distinct plateaus ((a) and (b) in Figure 5a) that could be identified and correspond to the two pairs of redox peaks in the CV plots. Another reversible phase transition occurs at  $2.99 \text{ V}$  vs  $\text{Li}^+/\text{Li}$ , assigned to the reversible transformation of  $\text{LiMn}_2\text{O}_4$  to  $\text{Li}_2\text{Mn}_2\text{O}_4$  [47] and this latter could have an effect on the cell performances. In contrast to the mentioned measurement, Kim *et al.* [48] performed cycling measurements for commercially available LMO in the voltage range of  $3.4\text{-}4.3 \text{ V}$ , and did not perceived the additional curve that appears for low voltage. Thus, the discharge and charge capacities were lower than the theoretical one of LMO, as displayed on Figure S7. Figure 5b exhibits the retention capacity, normalized with respect to the nominal one as a function of current scan for all calendered electrode films. The capacity retention decreases with increasing the current rate for all the samples, and this could be explained by the  $\text{Li}^+$  ion diffusion that occurs in the cathode material.



**Figure 5.** (a) Typical galvanostatic charge-discharge curve for  $\text{LiMn}_2\text{O}_4$  between 4.5 and 2.5 V vs  $\text{Li}^+/\text{Li}$ ; the inset refers to the CV plot of the same sample at  $0.5 \text{ mV s}^{-1}$ ; (b) capacity retention versus the current density xC with  $x=1, 2, 4, 6, 8$  and  $10$  for different calendered formulations .

Figure 6 exhibits the charge and discharge capacities collected for calendered films processed from 0 and 4 % of modified PVDF, cycled between 4.3 and 3.4 V vs Li<sup>+</sup>/Li. It can be noted that the formulation made with 4 wt.% of modified PVDF shows the best performance until 6 C, then similar behavior is perceived at 8 C, then a fade of the capacity was revealed at 10 C compared to the formulation made from commercial PVDF. The sample with 8 wt.% is the less performant. For instance, at 1 C, the initial charge capacities were 146, 140 and 130 mAh/g and decreased to 98, 88 and 80 mA h g<sup>-1</sup> at 10 C for films made by 0, 4 and 8 wt.% of modified PVDF, respectively. These findings could be explained by the PVDF content and its molar mass that are the main differences between the different samples. In fact, by adding 4 wt.% of modified PVDF, the electrochemical performances were more affected by the commercial PVDF that was predominant. However, a further increase in the modified PVDF, having a very low molar mass, led to low adhesion to current collector and thus induced a decrease in cell performances. Another possible reason for the fade of performances in the sample 8 wt.% could be due to the poor mechanical properties. In fact, the modified PVDF anchored onto BaTiO<sub>3</sub> nanoparticles is so brittle that it may induce a poor adherence onto the current collector.

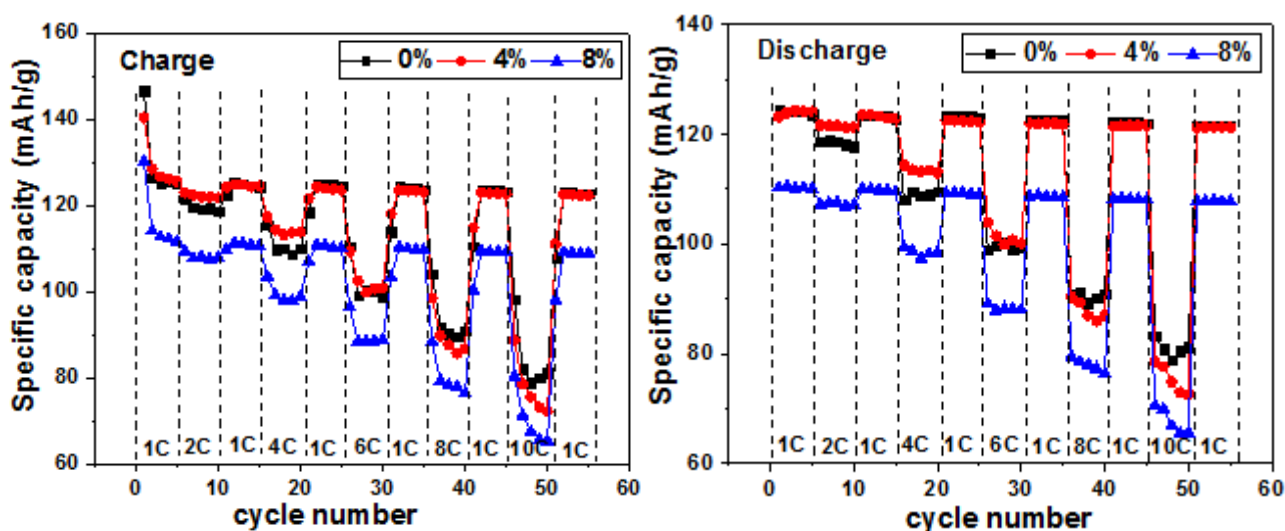


**Figure 6.** Charge and discharge capacities for calendered films processed from 0, 4 and 8 wt.% of modified PVDF, cycled between 4.3 and 3.4 V vs Li<sup>+</sup>/Li at different current densities.

#### 4. Conclusion

In this work, PVDF-*grafted*-Barium titanate (PVDF-*g*-BaTiO<sub>3</sub>) nanocomposites of various compositions were used as binders to prepare cathode material and their effects on the electrochemical performances were investigated. Four formulations were prepared by varying

the modified PVDF amount in the formulation starting from 0, 4, 8 and 12 % of PVDF-g-BaTiO<sub>3</sub>. Cells processed with 4 wt.% of modified PVDF showed similar cycling performances as the ones made from commercially available PVDF (0 wt.%) while the sample with 8 and 12 wt.% were less efficient in cycling. This could be explained by the low amount and the low molar mass of PVDF in the nanocomposites compared to that of the commercial one. On the other hand, and in order to obtain a uniform structure, the prepared films were calendered. This process induced an enhancement in cycling performances. For instance, the initial discharge capacity at 1C was 124 and 108 mAh/g, and decreased to 82 and 2 mAh/g at 10 C for calendered and non-calendered sample made with commercial PVDF, respectively. Thus, the calendering procedure proves to induce a positive effect on the cycling performances and is worth being applied. Moreover, PVDF with high molar mass is also desirable in order to favor a suitable binding of all the particles together on the current collector.

### **Acknowledgments**

The authors thank financial supports from the French Government (Campus France Maroc), *Centre National pour la Recherche Scientifique et Technique* in Morocco (CNRST (7UCA2016)) and Moroccan Ministry of High Education and Research Activities (MESRSFC) in the framework of *Centre d'Etudes Doctorales* (CEDoc) project. The French Fluorine network (GIS) is also acknowledged.

### **Notes and references**

- [1] L. Ramajo, M. Reboredo, M. Castro, Dielectric response and relaxation phenomena in composites of epoxy resin with BaTiO<sub>3</sub> particles, *Compos. Part A Appl. Sci. Manuf.* 36 (2005) 1267–1274. <https://doi.org/10.1016/J.COMPOSITESA.2005.01.026>.
- [2] Jiongxin Lu, C. Wong, Recent advances in high-k nanocomposite materials for embedded capacitor applications, *IEEE Trans. Dielectr. Electr. Insul.* 15 (2008) 1322–1328. <https://doi.org/10.1109/TDEI.2008.4656240>.
- [3] C.M. Costa, E. Lizundia, S. Lanceros-Méndez, Polymers for advanced lithium-ion batteries: State of the art and future needs on polymers for the different battery components, *Prog. Energy Combust. Sci.* 79 (2020) 100846. <https://doi.org/10.1016/j.peccs.2020.100846>.
- [4] L. Zhu, Q. Wang, Novel Ferroelectric Polymers for High Energy Density and Low Loss

- Dielectrics, *Macromolecules*. 45 (2012) 2937–2954. <https://doi.org/10.1021/ma2024057>.
- [5] Q. Wang, L. Zhu, *Polymer Nanocomposites for Electrical Energy Storage*, (2011) 1421–1429. <https://doi.org/10.1002/polb.22337>.
- [6] Prateek, V.K. Thakur, R.K. Gupta, Recent Progress on Ferroelectric Polymer-Based Nanocomposites for High Energy Density Capacitors: Synthesis, Dielectric Properties, and Future Aspects, *Chem. Rev.* 116 (2016) 4260–4317. <https://doi.org/10.1021/acs.chemrev.5b00495>.
- [7] X. Huang, P. Jiang, Core-Shell Structured High-k Polymer Nanocomposites for Energy Storage and Dielectric Applications, *Adv. Mater.* 27 (2015) 546–554. <https://doi.org/10.1002/adma.201401310>.
- [8] C. Sanchez, P. Belleville, M. Popall, L. Nicole, Applications of advanced hybrid organic–inorganic nanomaterials: From laboratory to market, *Chem. Soc. Rev.* 40 (2011) 696–753. <https://doi.org/10.1039/c0cs00136h>.
- [9] C. Yang, H. Wei, L. Guan, J. Guo, Y. Wang, X. Yan, X. Zhang, S. Wei, Z. Guo, Polymer nanocomposites for energy storage, energy saving, and anticorrosion, *J. Mater. Chem. A*. 3 (2015) 14929–14941. <https://doi.org/10.1039/c5ta02707a>.
- [10] X. Chen, Y. Zhao, L. Li, Y. Wang, J. Wang, J. Xiong, S. Du, P. Zhang, X. Shi, J. Yu, MXene/Polymer Nanocomposites: Preparation, Properties, and Applications, *Polym. Rev.* (2020) 1–36. <https://doi.org/10.1080/15583724.2020.1729179>.
- [11] K. Ding, H. Gu, C. Zheng, L. Liu, L. Liu, X. Yan, Z. Guo, Octagonal prism shaped lithium iron phosphate composite particles as positive electrode materials for rechargeable lithium-ion battery, *Electrochim. Acta*. 146 (2014) 585–590. <https://doi.org/10.1016/j.electacta.2014.08.141>.
- [12] A. Chakraborty, S. Kunnikuruvan, S. Kumar, B. Markovsky, D. Aurbach, M. Dixit, D.T. Major, Layered Cathode Materials for Lithium-Ion Batteries: Review of Computational Studies on  $\text{LiNi}_{1-x-y}\text{Co}_x\text{Mn}_y\text{O}_2$  and  $\text{LiNi}_{1-x-y}\text{Co}_x\text{Al}_y\text{O}_2$ , *Chem. Mater.* 32 (2020) 915–952. <https://doi.org/10.1021/acs.chemmater.9b04066>.
- [13] H. Zhang, C. Li, M. Piszcz, E. Coya, T. Rojo, L.M. Rodriguez-Martinez, M. Armand, Z. Zhou, Single lithium-ion conducting solid polymer electrolytes: Advances and

- perspectives, *Chem. Soc. Rev.* 46 (2017) 797–815. <https://doi.org/10.1039/c6cs00491a>.
- [14] J. Xu, S.L. Chou, Q.F. Gu, H.K. Liu, S.X. Dou, The effect of different binders on electrochemical properties of  $\text{LiNi}_{1/3}\text{Mn}_{1/3}\text{Co}_{1/3}\text{O}_2$  cathode material in lithium ion batteries, *J. Power Sources.* 225 (2013) 172–178. <https://doi.org/10.1016/j.jpowsour.2012.10.033>.
- [15] X. Cheng, J. Pan, Y. Zhao, M. Liao, H. Peng, Gel Polymer Electrolytes for Electrochemical Energy Storage, *Adv. Energy Mater.* 8 (2018) 1702184. <https://doi.org/10.1002/aenm.201702184>.
- [16] A. Kumar, R. Sharma, M.K. Das, P. Gajbhiye, K.K. Kar, Impacts of ceramic filler and the crystallite size of polymer matrix on the ionic transport properties of lithium triflate/poly (vinylidene fluoride-co-hexafluoropropene) based polymer electrolytes, *Electrochim. Acta.* 215 (2016) 1–11. <https://doi.org/10.1016/J.ELECTACTA.2016.08.087>.
- [17] P. Meneghetti, S. Qutubuddin, Synthesis, thermal properties and applications of polymer-clay nanocomposites, *Thermochim. Acta.* 442 (2006) 74–77. <https://doi.org/10.1016/j.tca.2006.01.017>.
- [18] S. Ferrari, J.R. Nair, Y. Zhou, C. Wan, Polymer nanocomposites for lithium battery applications, in: *Polym. Nanocomposites Energy Environ. Appl.*, Elsevier, 2018: pp. 283–313. <https://doi.org/10.1016/B978-0-08-102262-7.00010-6>.
- [19] S. Maazi, A.H. Navarchian, M. Khosravi, P. Chen, Effect of poly (vinylidene fluoride)/poly (vinyl acetate) blend composition as cathode binder on electrochemical performances of aqueous Li-ion battery, *Solid State Ionics.* 320 (2018) 84–91. <https://doi.org/10.1016/j.ssi.2018.02.033>.
- [20] N.-S. Choi, Y.-G. Lee, J.-K. Park, Effect of cathode binder on electrochemical properties of lithium rechargeable polymer batteries, *J. Power Sources.* 112 (2002) 61–66. [https://doi.org/10.1016/S0378-7753\(02\)00337-3](https://doi.org/10.1016/S0378-7753(02)00337-3).
- [21] P.P. Prosini, M. Carewska, A. Masci, A high voltage cathode prepared by using polyvinyl acetate as a binder, *Solid State Ionics.* 274 (2015) 88–93. <https://doi.org/10.1016/j.ssi.2015.03.008>.
- [22] S. Komaba, T. Ozeki, K. Okushi, Functional interface of polymer modified graphite

- anode, *J. Power Sources*. 189 (2009) 197–203.  
<https://doi.org/10.1016/j.jpowsour.2008.09.092>.
- [23] J. Chong, S. Xun, H. Zheng, X. Song, G. Liu, P. Ridgway, J.Q. Wang, V.S. Battaglia, A comparative study of polyacrylic acid and poly(vinylidene difluoride) binders for spherical natural graphite/LiFePO<sub>4</sub> electrodes and cells, *J. Power Sources*. 196 (2011) 7707–7714. <https://doi.org/10.1016/j.jpowsour.2011.04.043>.
- [24] V.H. Nguyen, W.L. Wang, E.M. Jin, H.B. Gu, Impacts of different polymer binders on electrochemical properties of LiFePO<sub>4</sub> cathode, *Appl. Surf. Sci.* 282 (2013) 444–449. <https://doi.org/10.1016/j.apsusc.2013.05.149>.
- [25] S.S. Jeong, N. Böckenfeld, A. Balducci, M. Winter, S. Passerini, Natural cellulose as binder for lithium battery electrodes, *J. Power Sources*. 199 (2012) 331–335. <https://doi.org/10.1016/j.jpowsour.2011.09.102>.
- [26] M.J. Lacey, F. Jeschull, K. Edstro, D. Brandell, Porosity Blocking in Highly Porous Carbon Black by PVDF Binder and Its Implications for the Li–S System, (2014). <https://doi.org/10.1021/jp508137m>.
- [27] A. Gören, C.M. Costa, M.M. Silva, S. Lanceros-Mendez, Influence of fluoropolymer binders on the electrochemical performance of C-LiFePO<sub>4</sub> based cathodes, *Solid State Ionics*. 295 (2016) 57–64. <https://doi.org/10.1016/j.ssi.2016.07.012>.
- [28] M. Zheng, X. Fu, Y. Wang, J. Reeve, L. Scudiero, W.-H. Zhong, Poly(Vinylidene Fluoride)-Based Blends as New Binders for Lithium-Ion Batteries, *ChemElectroChem*. 5 (2018) 2288–2294. <https://doi.org/10.1002/celec.201800553>.
- [29] M. Wang, J. Hu, Y. Wang, Y.-T. Cheng, The Influence of Polyvinylidene Fluoride (PVDF) Binder Properties on LiNi<sub>0.33</sub>Co<sub>0.33</sub>Mn<sub>0.33</sub>O<sub>2</sub> (NMC) Electrodes Made by a Dry-Powder-Coating Process, *J. Electrochem. Soc.* 166 (2019) A2151–A2157. <https://doi.org/10.1149/2.1171910jes>.
- [30] R. Wang, L. Feng, W. Yang, Y. Zhang, Y. Zhang, W. Bai, B. Liu, W. Zhang, Y. Chuan, Z. Zheng, H. Guan, Effect of Different Binders on the Electrochemical Performance of Metal Oxide Anode for Lithium-Ion Batteries, *Nanoscale Res. Lett.* 12 (2017). <https://doi.org/10.1186/s11671-017-2348-6>.

- [31] F.E. Bouharras, M. Raihane, G. Silly, C. Totee, B. Ameduri, Core shell structured Poly(Vinylidene Fluoride) -grafted- BaTiO<sub>3</sub> nanocomposites prepared via Reversible Addition fragmentation chain transfer (RAFT) polymerization of VDF for high energy storage capacitors, *Polym. Chem.* 10 (2019) 891–904.  
<https://doi.org/10.1039/C8PY01706A>.
- [32] C. Meyer, H. Bockholt, W. Haselrieder, A. Kwade, Characterization of the calendaring process for compaction of electrodes for lithium-ion batteries, *J. Mater. Process. Technol.* 249 (2017) 172–178. <https://doi.org/10.1016/j.jmatprotec.2017.05.031>.
- [33] C. Meyer, M. Kosfeld, W. Haselrieder, A. Kwade, Process modeling of the electrode calendaring of lithium-ion batteries regarding variation of cathode active materials and mass loadings, *J. Energy Storage.* 18 (2018) 371–379.  
<https://doi.org/10.1016/j.est.2018.05.018>.
- [34] C. Sangrós Giménez, B. Finke, C. Schilde, L. Froböse, A. Kwade, Numerical simulation of the behavior of lithium-ion battery electrodes during the calendaring process via the discrete element method, *Powder Technol.* 349 (2019) 1–11.  
<https://doi.org/10.1016/j.powtec.2019.03.020>.
- [35] H. Zheng, L. Tan, G. Liu, X. Song, V.S. Battaglia, Calendaring effects on the physical and electrochemical properties of Li[Ni 1/3Mn 1/3Co 1/3]O<sub>2</sub> cathode, *J. Power Sources.* 208 (2012) 52–57. <https://doi.org/10.1016/j.jpowsour.2012.02.001>.
- [36] Solef® PVDF Typical Properties, (n.d.). [https://www.solvay.jp/ja/binaries/Solef-PVDF-Typical-Properties\\_EN-229548.pdf](https://www.solvay.jp/ja/binaries/Solef-PVDF-Typical-Properties_EN-229548.pdf) (accessed April 29, 2020).
- [37] Y. Cai, Y. Huang, X. Wang, D. Jia, W. Pang, Z. Guo, Y. Du, X. Tang, Facile synthesis of LiMn<sub>2</sub>O<sub>4</sub> octahedral nanoparticles as cathode materials for high capacity lithium ion batteries with long cycle life, *J. Power Sources.* 278 (2015) 574–581.  
<https://doi.org/10.1016/j.jpowsour.2014.12.082>.
- [38] P. Ragupathy, H.N. Vasan, N. Munichandraiah, Microwave driven hydrothermal synthesis of LiMn<sub>2</sub>O<sub>4</sub> nanoparticles as cathode material for Li-ion batteries, *Mater. Chem. Phys.* 124 (2010) 870–875. <https://doi.org/10.1016/j.matchemphys.2010.08.014>.
- [39] H. Şahan, H. Göktepe, Ş. Patat, A Novel Method to Improve the Electrochemical Performance of LiMn<sub>2</sub>O<sub>4</sub> Cathode Active Material by CaCO<sub>3</sub> Surface Coating, *J. Mater.*

- Sci. Technol. 27 (2011) 415–420. [https://doi.org/10.1016/S1005-0302\(11\)60084-4](https://doi.org/10.1016/S1005-0302(11)60084-4).
- [40] D. Guo, B. Li, Z. Chang, H. Tang, X. Xu, K. Chang, E. Shangguan, X.Z. Yuan, H. Wang, Facile synthesis of  $\text{LiAl}_{0.1}\text{Mn}_{1.9}\text{O}_4$  as cathode material for lithium ion batteries: Towards rate and cycling capabilities at an elevated temperature, *Electrochim. Acta.* 134 (2014) 338–346. <https://doi.org/10.1016/j.electacta.2014.04.117>.
- [41] Y. Xia, H. Takeshige, H. Noguchi, M. Yoshio, Studies on an  $\text{LiMnO}$  spinel system (obtained by melt-impregnation) as a cathode for 4 V lithium batteries part 1. Synthesis and electrochemical behaviour of  $\text{Li}_x\text{Mn}_2\text{O}_4$ , *J. Power Sources.* 56 (1995) 61–67. [https://doi.org/10.1016/0378-7753\(95\)80009-6](https://doi.org/10.1016/0378-7753(95)80009-6).
- [42] F. Cheng, H. Wang, Z. Zhu, Y. Wang, T. Zhang, Z. Tao, J. Chen, Porous  $\text{LiMn}_2\text{O}_4$  nanorods with durable high-rate capability for rechargeable Li-ion batteries, *Energy Environ. Sci.* 4 (2011) 3668–3675. <https://doi.org/10.1039/c1ee01795k>.
- [43] C.F. Oladimeji, P.L. Moss, M.H. Weatherspoon, Analyses of the Calendaring Process for Performance Optimization of Li-Ion Battery Cathode, *Adv. Chem.* 2016 (2016) 1–7. <https://doi.org/10.1155/2016/7395060>.
- [44] A.M. Hashem, S.M. Abbas, X. Hou, A.E. Eid, A.E. Abdel-Ghany, Facile one step synthesis method of spinel  $\text{LiMn}_2\text{O}_4$  cathode material for lithium batteries, *Heliyon.* 5 (2019). <https://doi.org/10.1016/j.heliyon.2019.e02027>.
- [45] Y. Huang, H. Yang, Y. Zhang, Y. Zhang, Y. Wu, M. Tian, P. Chen, R. Trout, Y. Ma, T.-H. Wu, Y. Wu, N. Liu, A safe and fast-charging lithium-ion battery anode using MXene supported  $\text{Li}_3\text{VO}_4$ , (2019). <https://doi.org/10.1039/c9ta02037c>.
- [46] Q. Li, Q. Wei, J. Sheng, M. Yan, L. Zhou, W. Luo, R. Sun, L. Mai, Mesoporous  $\text{Li}_3\text{VO}_4/\text{C}$  Submicron-Ellipsoids Supported on Reduced Graphene Oxide as Practical Anode for High-Power Lithium-Ion Batteries, *Adv. Sci.* 2 (2015). <https://doi.org/10.1002/advs.201500284>.
- [47] J.M. Tarascon, D. Guyomard, Li Metal-Free Rechargeable Batteries Based on  $\text{Li}_{1+x}\text{Mn}_2\text{O}_4$  Cathodes ( $0 \leq x \leq 1$ ) and Carbon Anodes, *J. Electrochem. Soc.* 138 (1991) 2864–2868. <https://doi.org/10.1149/1.2085331>.
- [48] S. Kim, M. De Bruyn, J.G. Alauzun, N. Louvain, N. Brun, D.J. Macquarrie, L. Stievano,

B. Boury, L. Monconduit, P.H. Mutin, Alginic acid-derived mesoporous carbon (Starbon®) as template and reducing agent for the hydrothermal synthesis of mesoporous LiMn<sub>2</sub>O<sub>4</sub> grafted with carbonaceous species, *J. Mater. Chem. A*. 6 (2018) 14392–14399. <https://doi.org/10.1039/c8ta04128h>.

# Evaluation of core-shell poly(vinylidene fluoride)-*grafted*-Barium titanate (PVDF-*g*-BaTiO<sub>3</sub>) nanocomposites as a cathode binder in batteries

Fatima Ezzahra BOUHARRAS,<sup>a,b</sup> Mustapha RAIHANE,<sup>a</sup> Nicolas LOUVAIN,<sup>b</sup> Mohamed BACCOUR<sup>b</sup> and Bruno AMEDURI<sup>b</sup>

<sup>a</sup> Laboratory of Organometallic and Macromolecular Chemistry-Composite Materials (LCO2MC). Faculty of Sciences and Techniques, Cadi-Ayyad University, Av. Abdelkrim Khattabi, BP 549, 40000 Marrakesh, Morocco

<sup>b</sup> ICGM, Univ Montpellier, ENSCM, CNRS, Montpellier, France

